C. R. Mecanique 342 (2014) 539–557

Contents lists available at ScienceDirect

Comptes Rendus Mecanique

www.sciencedirect.com

Multi-directional and multi-time step absorbing layer for unbounded domain

Eliass Zafati *, Michaël Brun, Irini Djeran-Maigre, Florent Prunier

Université de Lyon, INSA-Lyon, LGCIE, 34, rue des Arts, 69621 Villeurbanne cedex, France

ARTICLE INFO

Article history:
Received 29 January 2014
Accepted 28 May 2014
Available online 27 June 2014

Keywords:
Unbounded medium
Absorbing layer
Subdomain coupling
Heterogeneous time integrators
Multi time steps

ABSTRACT

Variant techniques are proposed for reproducing the elastic wave propagation in an unbounded medium such as the infinite elements, the absorbing boundary conditions or the perfect matched layers. Here, a simplified approach is adopted by considering absorbing layers characterized by the viscous Rayleigh matrix as studied by Semblat et al. [16] and Rajagopal et al. [14]. Here, further improvements to this procedure are provided. First, we start by establishing the strong form for the elastic wave propagation in a medium characterized by the Rayleigh matrix. This strong form will be used for deriving optimal conditions for damping out in the most efficient way the incident waves while minimizing the spurious reflected waves at the interface between the domain of interest and the Rayleigh damping layer. A procedure for designing the absorbing layer is proposed by targeting a performance criterion expressed in terms of logarithmic decrement of the wave amplitude in the layer thickness. Second, the GC subdomain coupling method, proposed by Combescure and Gravouil [9], is introduced for enabling the choice of any Newmark time integration schemes associated with different time steps depending on subdomains. When wave propagation is predicted by an explicit time integrator, the subdomain strategy is of great interest because it enables a different time integrator for the absorbing layer to be adopted. An external coupling software, based on the GC method, is used to carry out multi=time step explicit/implicit co-computations, making interact in time an explicit FE code (Europlexus) for the domain of interest, with an implicit FE code (Cast3m) handling the absorbing boundary layers. The efficiency of the approach is shown in 1D and 2D elastic wave propagation problems.

1. Introduction

The simulation of the soil interaction problems [17] using the Finite Element method requires the modeling of unbounded media. Efficient numerical methods have to be set up, minimizing the number of operations while maintaining the accuracy of computation. For this purpose, the simplest way to achieve it is to use a very large model to prevent the numerical solution to be altered by the artificial reflected waves at the boundaries of the model. However, such a model becomes more costly in terms of computation time, especially when we work with complex structures in real configurations. In order to reduce the FE model, several methods have been developed by adding artificial conditions at the boundaries such as the

* Corresponding author.
E-mail addresses: eliass.zafati@insa-lyon.fr (E. Zafati), michael.brun@insa-lyon.fr (M. Brun), irini.djeran-maigre@insa-lyon.fr (I. Djeran-Maigre), florent.prunier@insa-lyon.fr (F. Prunier).

http://dx.doi.org/10.1016/j.crme.2014.05.007
1631-0721/

PML (Perfect Matched Layers) [3], absorbing boundaries [8], or infinite elements [4]. Though the aim of these techniques is to absorb all the incident energy without spurious wave reflections at the interface, some numerical disturbances appear when they are implemented in Finite Element codes. For example, Rajagopal et al. showed that the Perfect Matched Layers method suffers from numerical reflections at the interfaces [14] and instabilities [12].

One of the simplest techniques for absorbing incident waves is to introduce viscous layers characterized by the Rayleigh matrix at the boundaries. This technique was already used with different approaches [16,14] and turns out to be efficient and easy to implement. However, the amount of spurious waves reflected at the interfaces is not easy to be predicted as well as the optimal thickness for achieving an acceptable efficiency.

The use of the Rayleigh matrix for soil dynamics problems is not straightforward because the behavior of the derived Rayleigh material can be viewed as unphysical. However, Semblat et al. give a rheological interpretation of this material [15].

When addressing the numerical implementation, it is important to underline that the introduction of the Rayleigh matrix decreases the value of the critical time step when using the explicit scheme, impinging the computation time [14]. In addition, in a FE code based on the explicit time integration scheme (central difference method), the viscous damping can only be introduced by employing the mass matrix. It is interesting to be able to adopt a classical Rayleigh matrix for only absorbing layers, built from the mass and stiffness matrices, by using an implicit time integration scheme such as the average acceleration method. The subdomain method proposed by Gravouil and Combescure [7] provides the suitable properties for coupling an explicit integrator for the subdomain of interest with an implicit one for the absorbing layers. The method follows a dual Schur approach by ensuring the velocity continuity at the interface through Lagrange multipliers. The method is proved to be stable for any Newmark integrators using the so-called energy method (Hughes [10]). It leads to the first order of accuracy when coupling second-order accurate time integration schemes due to a slight spurious dissipation at the interface as soon as different time steps are adopted. When adopting the same time step, the second order of accuracy is achieved. In this work, heterogeneous time steps are considered, leading to a first accurate multi time step coupling scheme. Co-computations will be carried out by using an external software based on the GC method, coupling an explicit FE code with an implicit one, validated against full explicit computation with a homogeneous time step for reinforced concrete structures subjected to earthquake excitations [5,6].

In this present paper, the technique of the absorbing layers by using the Rayleigh matrix is adopted. Next, we suggest to:

1. Show the link between the Rayleigh matrix and the Kelvin–Voigt model. Consequently, we will give a strong form of the wave propagation problem in the absorbing layer in order to optimize the parameters required for designing the absorbing layer. This optimization is based on harmonic waves.
2. Present a multi-layer strategy that will be used as an alternative method to the previous one using a single absorbing layer. The main idea consists in dividing the damping subdomain into several sublayers, each one with their own parameters. The aim is to reduce the scale of the whole absorbing layer.
3. Validate the analytical developments in the previous parts by considering numerical examples: first without subdomain decomposition for a 1D wave propagation problem, and second, with the GC coupling method using different time steps for 2D Lamb's problem [11]: the domain of interest will be integrated in time with a central difference scheme associated with a fine time step, whereas the absorbing layers will be dealt with an average acceleration scheme related to a large time step in order to reduce the computation time devoted to the modeling of the unbounded medium. Two different finite-element codes will be involved in the multi time step explicit/implicit co-computations: Europlexus [2] based on the explicit scheme (Central Difference) and Cast3m [1] based on the implicit scheme (Average Acceleration). The multi-layer strategy will be compared with the analytical expressions for Lamb's test.

2. Dissipative medium characterized by a Rayleigh matrix

We study the wave propagation from a non-dissipative medium to a dissipative one. The dissipative medium plays the role of the absorbing layer to damp out the incident waves coming from the domain of interest in order to reproduce the unbounded conditions. Using the Finite Element Method for discretizing in space the media, the classical Rayleigh damping is adopted in the dissipative medium as proposed by Semblat et al. [16] and Rajagopal et al. [14]. This simple choice is convenient because it is available in any Finite Element packages. Nonetheless, it introduces spurious wave reflections at the interface between the two subdomains. The design of the absorbing layer is done by numerical experiments by reducing the spurious reflections to an acceptable level. In this paper, a strong form of the wave propagation in the continuous dissipative medium is proposed. After writing the problem into its weak form and discretizing it through the Finite Element Method, it will be shown that it corresponds to the introduction of the Rayleigh matrix into the classical space discretization of the equation of motion. The interest of the strong form for wave propagation in the dissipative medium, characterized by a Rayleigh matrix in its discrete form, lies in the fact that it enables a proper design for the absorbing layer. Indeed, once obtained the strong form for wave propagation in the Rayleigh damping medium, the interface problem can be analytically studied by writing the continuity of displacements and the stress equilibrium at the interface. As a result, the spurious reflections at the boundaries of the domain of interest will be reduced by adapting the material parameters of the absorbing layer so as to cancel out the reflection coefficient for the 1D propagation problem with harmonic waves. It will be shown later that the derived relationship for minimizing the spurious reflections at the interface in the case of 1D harmonic waves

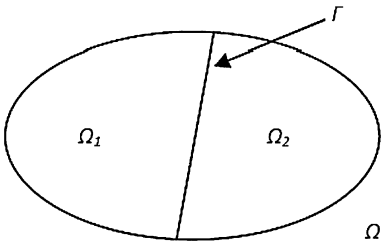

Fig. 1. Domain Ω divided into two subdomains Ω_1 and Ω_2.

provides also good results in more general cases (non-harmonic waves, non-normal, composed of body and surface waves). In addition, the thickness of the absorbing layer will be obtained as a function of a target performance value expressed in terms of total logarithmic decrement for the incident waves. Finally, time discretization of the coupled problem is presented by following a subdomain strategy proposed by Gravouil and Combescure [7], enabling to choose different time integrators and time steps in the non-dissipative and dissipative media.

2.1. The boundary value problem (strong form)

Let Ω a bounded domain from $\mathbb{R}^3$ with a regular boundary. We assume that the domain Ω is divided into two parts Ω_1 and Ω_2, as illustrated in Fig. 1, such as: $\Omega_1 \cap \Omega_2 = \oslash$ and $\partial\Omega_1 \cap \partial\Omega_2 = \Gamma$. Γ represents the interface between the two subdomains: subdomain Ω_1 related to a non-dissipative linear elastic behavior and subdomain Ω_2 related to a dissipative behavior characterized in the following. A linear elastic behavior is assumed for both subdomains, with an infinitesimal strain tensor defined by:

$$\epsilon(u) = \frac{1}{2}\left(\nabla u + \nabla^{\mathrm{t}} u\right) \tag{1}$$

u being the field displacement vector.

Subdomain Ω_1:

It is assumed that medium Ω_1 is linear elastic, characterized by density ρ_1 and Lamé's coefficients λ_1 and μ_1. E_1 and ν_1 are Young's modulus and Poisson's coefficient of this material. The boundary conditions are given by:

$$\begin{cases} \sigma \cdot n_1 = g_{1n} \quad \text{on } \partial\Omega_{1n} \\ u_1 = u_{1d} \quad \text{on } \partial\Omega_{1d} \end{cases} \tag{2}$$

Here, $\partial\Omega_{1d}$ and $\partial\Omega_{1n}$ are parts of the boundary with $\partial\Omega_{1n} \cup \partial\Omega_{1d} = \partial\Omega_1 \setminus \Gamma$ and $\partial\Omega_{1n} \cap \partial\Omega_{1d} = \oslash$.

The initial conditions are:

$$\begin{cases} u_1(x \in \Omega_1, t = 0) = 0 \\ \partial_t u_1(x \in \Omega_1, t = 0) = 0 \end{cases} \tag{3}$$

Subdomain Ω_2:

We assume that the displacement vector field u_2 is governed by the following equations:

$$\rho_2 \partial_t^2 u_2 + a\rho_2 \partial_t u_2 = \operatorname{div}\left(\sigma_2(u_2)\right) \tag{4}$$

$$\sigma_2 = \lambda_2 \operatorname{tr}\left(\epsilon(u_2)\right) + 2\mu_2 \epsilon(u_2) + b\left(\lambda_2 \operatorname{tr}\left(\epsilon(\partial_t u_2)\right) + 2\mu_2 \epsilon(\partial_t u_2)\right) \tag{5}$$

with a, b, λ_2, μ_2 being positive integers.

Eq. (5) defines a viscous Kelvin–Voigt material with b corresponding to the characteristic time parameter. From Eq. (4), it can be seen that a dashpot corresponding to a viscous term has been added on the left-hand side of the continuous equation of motion in its strong form. The added viscous term is characterized by the damping coefficient $a\rho_2$. Parameters λ_2, μ_2 are Lamé's coefficients. Similarly, E_2 and ν_2 are the Young modulus and the Poisson ratio of the viscous Kelvin–Voigt material. It will be shown in the following that the strong form given in Eqs. (4) and (5) leads to the classical semi-discretized equation of motion with a Rayleigh damping matrix.

Particular boundary conditions are given as follows:

$$\sigma_2 . n_2 = 0 \quad \text{on } \partial\Omega_{2n} \qquad u_2 = 0 \quad \text{on } \partial\Omega_{2d} \tag{6}$$

with

$$\partial\Omega_{2n} \cup \partial\Omega_{2d} = \partial\Omega_2 \setminus \Gamma \qquad \partial\Omega_{2n} \cap \partial\Omega_{2d} = \oslash \tag{7}$$

The initial conditions are taken as:

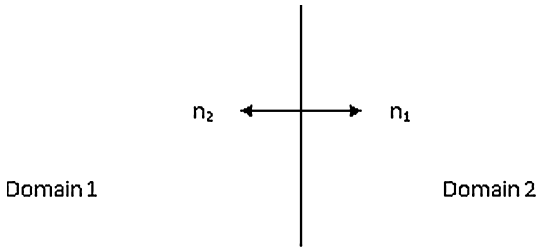

Fig. 2. Conventional normal vectors at the interface.

$$u_2(x \in \Omega_2, t=0) = 0 \qquad \partial_t u_2(x \in \Omega_2, t=0) = 0 \tag{8}$$

The interface

Fig. 2 illustrates the conventional orientations of the normal vectors. The continuity of displacements and equilibrium of stresses are given by:

$$\sigma_2.n_2 = -\sigma_1.n_1 \quad \text{on } \Gamma; \qquad u_1 = u_2 \quad \text{on } \Gamma \tag{9}$$

2.2. Space discretization of the split domain

For the purpose of approximating the solution of the previous equations in their strong form by the Finite Element Method, we have first to write the problem into its weak form. Then the classical shape functions will be introduced in order to derive the semi-discretized equations of motion for the domain Ω split into two subdomains Ω_1 and Ω_2.

We start by giving some definitions of the test function spaces:

$$E_1 = \left\{ v_1 \in C_c^\infty(\overline{\Omega}) / v_1 = 0 \text{ on } \partial\Omega_{1d} \right\}$$
$$E_2 = \left\{ v_2 \in C_c^\infty(\overline{\Omega}) / v_2 = 0 \text{ on } \partial\Omega_{2d} \right\}$$

We assume that $u_1 \in H^2(\Omega)$, by applying the Green formula for each test function $v_1 \in E_1$:

$$\int_{\Omega_1} \rho_1 \partial_t^2 u_1 \cdot v_1 \, \mathrm{d}\Omega_1 + \int_{\Omega_1} \sigma_1 \cdot \epsilon(v_1) \, \mathrm{d}\Omega_1 = \int_{\partial\Omega_{1n}} g_{1n} \cdot v_1 \, \mathrm{d}\Omega_{1n} + \int_{\Gamma} (\sigma_1.n_1) \cdot v_1 \, \mathrm{d}\Gamma \tag{10}$$

We also assume that $u_2 \in H^2(\Omega)$ and $\partial_t u_2 \in H^2(\Omega)$. Again the Green formula is applied for each test function $v_2 \in E_2$:

$$\int_{\Omega_2} \rho_2 \partial_t^2 u_2 \cdot v_2 \, \mathrm{d}\Omega_2 + \int_{\Omega_2} \sigma_2 \cdot \epsilon(v_2) \, \mathrm{d}\Omega_2 + a \int_{\Omega_2} \rho_2 \partial_t u_2 \cdot v_2 \, \mathrm{d}\Omega_2 = \int_{\Gamma} (\sigma_2 \cdot n_2) \cdot v_2 \, \mathrm{d}\Gamma \tag{11}$$

Let u_{1h}, u_{2h}, v_{1h} and v_{2h} (h being representing the size of the element) be the approximate vectors related to the continuous displacement fields u_1, u_2, v_1 and v_2, respectively. The approximate solution is written according to each element e for the first domain Ω_1 as: $u_{1h}^e = N_1^e U_1^e$, with N_1^e corresponding to the shape function matrix and U_1^e the nodal displacement vector related to the element e. Similarly, we write: $u_{2h}^e = N_2^e U_2^e$, $v_{1h}^e = N_1^e V_1^e$ and $v_{2h}^e = N_2^e V_2^e$.

Concerning the continuity condition at the interface between subdomains, the method proposed by Gravouil and Combescure [7] is employed. It is based on a dual Schur approach by introducing Lagrange multipliers to ensure the kinematic continuity at the interface. When discretizing in time the equation of motion for both subdomains, we have to choose the quantity (displacement, velocity or acceleration) whose continuity is imposed at the interface. Following the GC method, it has been proven by the authors that any Newmark time integrators can be coupled (for example, explicit central difference scheme with implicit average acceleration scheme) when the continuity of velocities at the interface is prescribed. Thus it has been assumed the following constraint on velocities at the interface:

$$L_1 \dot{U}_1 + L_2 \dot{U}_2 = 0 \tag{12}$$

where L_1 and L_2 are the Boolean matrices, operating on nodal vectors associated with the two subdomains Ω_1 and Ω_2, and picks out the degrees of freedom lying on the interface Γ.

Furthermore, the virtual work at the interface on the right-hand side of the weak forms in Eq. (10) and Eq. (11) can be expressed as:

$$\begin{cases} \displaystyle\int_{\Gamma} (\sigma_1 \cdot n_1) \cdot v_1 \, \mathrm{d}\Gamma = -V_1^{\mathrm{T}} L_1^{\mathrm{T}} \hat{\lambda}(t) \\ \displaystyle\int_{\Gamma} (\sigma_2 \cdot n_2) \cdot v_2 \, \mathrm{d}\Gamma = -V_2^{\mathrm{T}} L_2^{\mathrm{T}} \hat{\lambda}(t) \end{cases} \tag{13}$$

$\hat{\lambda}(t)$ being the Lagrange multiplier vector corresponding to the nodal forces at the interface.

We assume that the problem presented above has one unique solution. Through the weak formulation and the classical arguments of the Finite Element approximation [10], the problem in the discretized space in subdomain Ω_1 is given by:

$$M_1\ddot{U}_1 + K_1U_1 = F_1^{\text{ext}} - L_1^{\text{T}}\hat{\lambda} \tag{14}$$

and in subdomain Ω_2:

$$M_2\ddot{U}_2 + K_2U_2 + (aM_2 + bK_2)\dot{U}_2 = -L_2^{\text{T}}\hat{\lambda} \tag{15}$$

Here M_i and K_i are the mass and the stiffness matrices related to subdomains Ω_1 and Ω_2. It can be recognized in the semi-discretized Eq. (15) the classical Rayleigh damping matrix noted as: $C_2 = aM_2 + bK_2$, where a and b are the constants usually chosen so as to match the damping ratio at two specific frequencies. Thus it has been shown that the strong forms proposed in Eqs. (4) and (5) are related to the classical semi-discretized equation of motion with the introduction of the Rayleigh damping matrix governing the behavior of subdomain Ω_2. The advantage of the strong form governing the behavior of a Rayleigh medium lies in fact that it can be easily employed in order to better describe the propagative properties of the Rayleigh medium and determine some conditions for minimizing the reflected waves at the interface. Furthermore, it enables the absorbing layer to be properly designed by investigating the two following points: the dissipative capability into the absorbing layer and the level of spurious reflections at the interface.

2.3. Time discretization of the coupled problem

The time integration of the coupled system composed of the previous semi-discretized equations is dealt following the GC method [7]. Newmark time integration schemes are considered for both subdomains. The acceleration format is adopted. Considering a time step $\Delta t = [t_n; t_{n+1}]$, the displacements and velocities at the end of the time step are approximated as:

$$U_k^{n+1} = U_k^{n,p} + \beta\Delta t^2\ddot{U}_k^{n+1} \tag{16}$$

$$\dot{U}_k^{n+1} = \dot{U}_k^{n,p} + \gamma\Delta t\ddot{U}_k^{n+1} \tag{17}$$

(β, γ) are the parameters of the Newmark scheme. $U_k^{n,p}$ and $\dot{U}_k^{n,p}$ are the predictor quantities, determined from the quantities known at the beginning of time step as:

$$U_k^{n,p} = U_k^n + \Delta t\,\dot{U}_k^n + \Delta t^2\left(\frac{1}{2} - \beta\right)\ddot{U}_k^n \tag{18}$$

$$\dot{U}_k^{n,p} = \dot{U}_k^n + \Delta t(1-\gamma)\,\ddot{U}_k^n \tag{19}$$

As mentioned before, the authors proved that imposing velocity continuity enables any Newmark time integrators to be selected. Next subdomain Ω_1 is integrated in time with an explicit time integration scheme (central difference scheme), characterized by the parameters $\gamma_1 = 0.5$ and $\beta_1 = 0$, whereas subdomain Ω_2 is handled with an implicit time integration scheme (constant acceleration scheme), characterized by parameters $\gamma_2 = 0.5$ and $\beta_2 = 0.25$. Note that the main advantage of the coupling GC method is to provide heterogeneous time integration and multi-time step capabilities. The multi time step ability is of great interest for minimizing the computation time required in the absorbing layer while keeping a target accuracy in the subdomain of interest. Here we seek to design an absorbing layer associated with a damping Rayleigh matrix by minimizing the spurious reflections at the interface due to the different damping properties of the subdomains under consideration. We focus on heterogeneous time integration of the coupled problem by using different time steps in the two subdomains. For this purpose, we define the fine time scale Δt_1 for the explicit domain and the coarse time scale Δt_2 for the implicit domain with $\Delta t_2 = m\Delta t_1$. The equilibrium of subdomain 1 is prescribed at time $t_m = \Delta t_2$, while the equilibrium of subdomain 2 is prescribed at time $t_j = j\Delta t_1$ $(j = 1, 2, \ldots, m)$ as follows:

- subdomain 1:

$$M_1\ddot{U}_1^j + K_1U_1^j = F_1^{ext,j} - L_1^T\hat{\lambda}^j \tag{20}$$

- subdomain 2:

$$M_2\ddot{U}_2^m + C_2\dot{U}_2^m + K_2U_2^m = -L_2^T\hat{\lambda}^m \tag{21}$$

At the interface, the continuity of velocities is imposed at time t_j as:

$$L_1\dot{U}_1^j + L_2\dot{U}_2^j = 0 \tag{22}$$

Using the expressions of the kinematic quantities in Eqs. (16) and (17), the equilibrium equations can be written in the form:

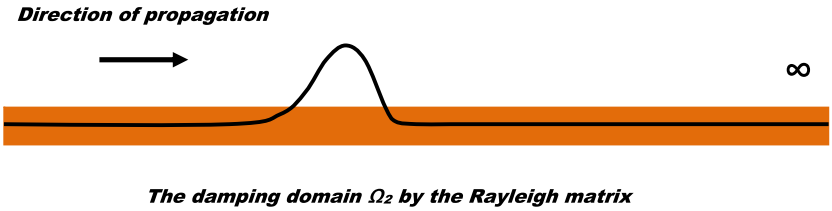

Fig. 3. (Color online.) The problem of the wave propagation in 1D medium.

$$\widetilde{M}_1 \ddot{U}_1^j = F_1^{\text{ext},j} - K_1 U_1^{j-1,p} - L_1^T \hat{\lambda}^j \tag{23}$$

$$\widetilde{M}_2 \ddot{U}_2^m = F_2^{\text{ext},m} - C_2 \dot{U}_2^{0,p} - K_2 U_2^{0,p} - L_2^T \hat{\lambda}^m \tag{24}$$

with the effective stiffness matrices defined by:

$$\widetilde{M}_1 = M_1 + \beta_1 \Delta t_1^2 K_1 \tag{25}$$

$$\widetilde{M}_2 = M_2 + \beta_2 \Delta t_2^2 K_1 + \gamma_2 \Delta t C_2 \tag{26}$$

The procedure proposed by Gravouil and Combescure is based on splitting the kinematic quantities into two parts: the free and the linked quantities. The free quantities are obtained by only considering the internal and external forces, whereas the linked quantities are obtained by taking into account only the interface loads defined by the Lagrange multiplier vector $\hat{\lambda}$. For example, if we consider subdomain Ω_2, the discrete equation of motion is split into two parts as follows:

$$\begin{cases} \widetilde{M}_2 \ddot{U}_2^{\text{free},m} = F_2^{\text{ext},m} - C_2 \dot{U}_2^{0,p} - K_2 U_2^{0,p} \\ \widetilde{M}_2 \ddot{U}_2^{\text{link},m} = -L_2^{\text{T}} \hat{\lambda}^m \end{cases} \tag{27}$$

The complete accelerations are obtained by summing the two parts as: $\ddot{U}_2^m = \ddot{U}_2^{\text{free},m} + \ddot{U}_2^{\text{link},m}$.

The same procedures are applied to subdomain Ω_1 at each time t_j. Furthermore, the kinematic quantities of subdomain 2 at t_j are interpolated as well as the Lagrange multiplier:

$$\begin{cases} \hat{\lambda}^j = \left(1 - \dfrac{j}{m}\right)\hat{\lambda}^0 + \dfrac{j}{m}\hat{\lambda}^m \\ W_2^j = \left(1 - \dfrac{j}{m}\right) W_2^0 + \dfrac{j}{m} W_2^m \end{cases} \tag{28}$$

Here W_2^j can be either the free or the linked kinematic quantities of subdomain 2 at t_j. Using the kinematic condition at the interface in Eq. (22) at each time t_j, we obtain:

$$L_1 \dot{U}_1^{\text{link},j} + L_2 \dot{U}_2^{\text{link},j} = -L_1 \dot{U}_1^{\text{free},j} - L_2 \dot{U}_2^{\text{free},j} \tag{29}$$

Then, by using Eq. (28) and the expression of the velocities as a function of accelerations, the following interface problem can be derived:

$$H \hat{\lambda}^j = b_j \tag{30}$$

with the interface operator and the second side member vector defined by:

$$\begin{cases} H = \gamma_1 \Delta t L_1 \widetilde{M}_1^{-1} L_1^{\text{T}} + \gamma_2 \Delta t L_2 \widetilde{M}_2^{-1} L_2^{\text{T}} \\ b_j = -L_1 \dot{U}_1^{\text{free},j} - L_2 \dot{U}_2^{\text{free},j} \end{cases} \tag{31}$$

Finally, once we get the values of the Lagrange multiplier vector at the end time of the time step, linked accelerations are obtained and thus complete accelerations as well as displacements and velocities from Newmark formulae in Eqs. (16) and (17).

3. Wave propagation in Rayleigh damping medium and at the interface

3.1. 1D wave propagation in the Rayleigh medium

In this part, the wave propagation problem is studied in 1D medium related to the Rayleigh matrix characterized by the two parameters a and b. We assume that the medium is infinite and the wave propagates according to the direction of e_x (Fig. 3).

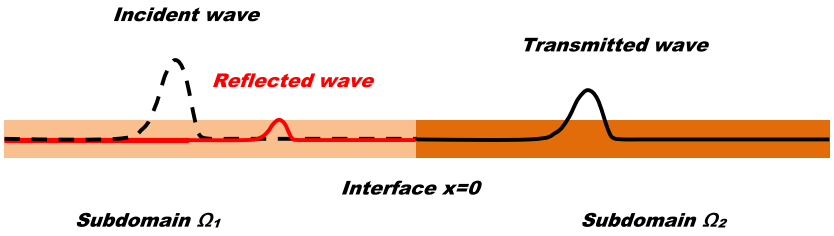

Fig. 4. (Color online.) Wave propagation in two media separated by an interface $x = 0$.

3.1.1. Harmonic waves

Since the problem is 1D, the displacement can be put in the form: $u_2(x,t) = \widetilde{u}_2(x,t)e_x$ for P-waves or $u_2(x,t) = \widetilde{u}_2(x,t)e_z$ for S-waves.

The propagation wave equations for P-waves and S-waves in their strong form, given in Eq. (4), can be simplified as:

$$\rho_2\partial_t^2\widetilde{u}_2 + a\rho_2\partial_t\widetilde{u}_2 = (\lambda_2+2\mu_2)\partial_x^2\widetilde{u}_2 + b(\lambda_2+2\mu_2)\partial_x^2\partial_t\widetilde{u}_2 \quad \text{P-waves} \tag{32}$$

$$\rho_2\partial_t^2\widetilde{u}_2 + a\rho_2\partial_t\widetilde{u}_2 = \mu_2\partial_x^2\widetilde{u}_2 + b\mu_2\partial_x^2\partial_t\widetilde{u}_2 \quad \text{S-waves} \tag{33}$$

We start by considering harmonic solutions for the above equations written in the following form:

$$\widetilde{u}_2(x,t) = T\exp\big(\mathrm{i}(\omega_0 t - kx)\big) \tag{34}$$

with k the wave number assumed to be a complex such as: $Re(k) \geq 0$.

By introducing this solution into the previous propagation wave equations in Eqs. (32) and (33), we obtain the expression of the wave number k:

$$k^2 = \left(\frac{\omega_0}{V_2}\right)^2 \frac{1 - ab - \mathrm{i}(\frac{a}{\omega_0} + b\omega_0)}{1 + b^2\omega_0^2} \tag{35}$$

with the phase velocity V_2 equal to $\sqrt{\frac{\lambda_2+2\mu_2}{\rho_2}}$ for P-waves and $\sqrt{\frac{\mu_2}{\rho_2}}$ for S-waves. We remark that the expression of k is a complex number depending on two parameters a and b. It is convenient to choose them as:

$$\frac{a}{\omega_0} = b\omega_0 = \xi \tag{36}$$

ξ being the damping ratio.

Finally, we get the expression of the propagating wave in the 1D medium damped by a Rayleigh matrix:

$$\widetilde{u}_2(x,t) = T\exp\left(\frac{-\omega_0\xi x}{V_2\sqrt{1+\xi^2}}\right)\exp\left(\mathrm{i}\left(\omega_0 t - \frac{\omega_0 x}{V_2\sqrt{1+\xi^2}}\right)\right) \tag{37}$$

The logarithmic decrement is defined as: $\delta = \ln(\frac{|\widetilde{u}_2|(x)}{|\widetilde{u}_2|(x+\Delta x)})$. It quantifies the decay of the amplitude of the propagating wave into the 1D damped medium when it travels through a distance Δx. Using the previous expression of the propagating wave, the relationship between the logarithmic decrement and the distance is given by:

$$\Delta x = \frac{V_2}{\omega_0}\frac{\delta\sqrt{1+\xi^2}}{\xi} \tag{38}$$

The above relationship will be used for the design of the absorbing layer associated with a Rayleigh matrix: starting from a target value for the logarithmic decrement, the thickness of the absorbing layer Δx can be easily derived.

3.2. 1D wave propagation from an elastic medium to a Rayleigh medium

This section is devoted to the study of the propagation of harmonic and non-harmonic 1D waves from an elastic medium to the damped medium characterized by the Raleigh matrix in its discrete formulation. Again the strong forms for the wave propagation are considered. By writing the continuity of displacements and equilibrium of stresses at the interface, it will be shown that conditions on material properties of the Rayleigh medium can be derived so as to cancel out the reflected waves in the case of 1D harmonic waves.

Let us consider an elastic linear medium Ω_1 and a Rayleigh medium Ω_2. We assume harmonic waves (P-wave or S-wave), propagating from Ω_1 towards Ω_2, as shown in Fig. 4.

The wave propagation problem is 1D and the main purpose is to quantify the spurious waves created at the interface.

3.2.1. Harmonic waves

Let us introduce $\widetilde{u}_1$ the incident wave, $\widetilde{u}_2$ the transmitted wave and $\widetilde{u}_{\mathrm{R}}$ the reflected wave. Using the same values of the parameters a and b as done in Eq. (36), we write:

$$\widetilde{u}_1(x,t) = A\exp\left(\mathrm{i}\omega_0\left(t - \frac{x}{V_1}\right)\right) \tag{39}$$

$$\widetilde{u}_2(x,t) = T\exp\left(\frac{-\omega_0\xi x}{V_2\sqrt{1+\xi^2}}\right)\exp\left(\mathrm{i}\left(\omega_0 t - \frac{\omega_0 x}{V_2\sqrt{1+\xi^2}}\right)\right) \tag{40}$$

$$\widetilde{u}_R(x,t) = R\exp\left(\mathrm{i}\omega_0\left(t + \frac{x}{V_1}\right)\right) \tag{41}$$

where V_i $\{i=1,2\}$ is the phase velocity and is equal to $\sqrt{\frac{\lambda_i+2\mu_i}{\rho_i}}$ for P-waves and $\sqrt{\frac{\mu_i}{\rho_i}}$ for S-waves.

From the continuous conditions at the interface (continuity of displacements and equilibrium of stresses), we have:

$$\widetilde{u}_2(x=0,t) = \widetilde{u}_1(x=0,t) + \widetilde{u}_{\mathrm{R}}(x=0,t) \tag{42}$$

$$\kappa_2\partial_x\widetilde{u}_2(x=0,t) = \kappa_1(\partial_x\widetilde{u}_1 + \partial_x\widetilde{u}_{\mathrm{R}})(x=0,t) \tag{43}$$

with κ_i $\{i=1,2\}$ being equal to $\lambda_i+2\mu_i$ for P-waves or $2\mu_i$ for S-waves.

We focus on the reflected waves generated at the interface. Using the expressions of the involved waves in Eqs. (39) to (41) and the previous interface relationships, the reflection coefficient can be obtained as:

$$\frac{R}{A} = \frac{1-\gamma\sqrt{1+\xi^2}}{1+\gamma\sqrt{1+\xi^2}} \tag{44}$$

with parameter γ defined by: $\gamma = \frac{\rho_2 V_2}{\rho_1 V_1}$.

Now, we can give a condition under which the reflected P-waves and S-waves vanish as follows:

$$\gamma = \frac{1}{\sqrt{1+\xi^2}} \tag{45}$$

For two subdomains, by choosing $\rho_1 = \rho_2$, the zero interface reflection coefficient condition writes as:

$$\begin{cases} \lambda_2 = \dfrac{\lambda_1}{1+\xi^2} & \mu_2 = \dfrac{\mu_1}{1+\xi^2} \\ E_2 = \dfrac{E_1}{1+\xi^2} & \nu_2 = \nu_1 \end{cases} \tag{46}$$

The results given by Eq. (46) show the relationships between Young's modulus and Poisson's ratio for each material composing the subdomains separated by an interface. This condition is sufficient for canceling out the reflected wave in the case of 1D harmonic waves. For non-harmonic waves with a dominant frequency, this condition will be further used as an approximation.

3.3. Multi-layer strategy

The problem of 1D wave propagation through media with different viscous damping characteristics is investigated. By writing the displacement continuity and the stress equilibrium at the interface, the conditions to eliminate the reflected waves in the case of 1D harmonic waves are given by:

$$\begin{cases} \dfrac{E_2^{(1)}}{E_2^{(2)}} = \dfrac{1+\xi_2^2}{1+\xi_1^2} \\ \nu_2^{(1)} = \nu_2^{(2)} \end{cases} \tag{47}$$

$E_2^{(1)}$, $E_2^{(1)}$, $\nu_2^{(1)}$ and $\nu_2^{(2)}$ being the Young moduli and Poisson coefficients of the two sublayers (1) and (2).

Now we consider a series of N absorbing sublayers with different damping ratios ξ_i related to sublayer (i), $1 \le i \le N$. We denote also $E_2^{(i)}$ the Young modulus and $\nu_2^{(i)}$ the Poisson coefficient of sublayer (i). Assuming a homogeneous density for all the sublayers, the following conditions are imposed:

$$\begin{cases} E_2^{(i+1)} = \frac{1+\xi_i^2}{1+\xi_{i+1}^2} E_2^{(i)} \\ E_2^{(1)} = \dfrac{1}{1+\xi_1^2} E_1 \\ \nu_2^{(i)} = \nu_1 \\ \xi_{i+1} - \xi_i = a \end{cases} \tag{48}$$

where a is a positive integer, representing the damping increase between two sublayers.

In order to avoid important spurious waves at the interface between the domain of interest and the total absorbing layer, the first damping ratio ξ_1 has to be chosen weak enough as well as the parameter a defining the step between two consecutive damping ratios. We call e_i the thickness of each sublayer and e the total thickness of the total absorbing layer composed of N sublayers. Similarly, we denote δ_i the logarithmic decrement associated with each sublayer and δ the logarithmic decrement of the total absorbing layer. We have the following relationships:

$$\sum_{i=1}^{N} e_i = e \qquad \sum_{i=1}^{N} \delta_i = \delta \tag{49}$$

From Eq. (38) giving the distance related to a target logarithmic decrement δ_i, the thickness of the sublayer can be expressed as:

$$e_i = \frac{V_{2p}^{(i)}}{\omega_0} \frac{\delta_i \sqrt{1+\xi_i^2}}{\xi_i} \tag{50}$$

Finally, we write the system in the form:

$$\begin{cases} \displaystyle\sum_{i=1}^{N} e_i = e \\ \dfrac{\omega_0}{V_{1p}} \displaystyle\sum_{i=1}^{N} \xi_i e_i = \delta \\ \xi_{i+1} - \xi_i = a \end{cases} \tag{51}$$

Given the constraint on the element size h usually selected to be constant in the whole mesh, it is necessary to set the thickness of each sublayer according to this element size. To simplify, we choose h as the thickness of each sublayer (one element per sublayer) and we calculate the total number of the sublayers N using the system in Eq. (51) and the target value of the logarithmic decrement δ. The damping ratio ξ_i is, of course, constant in each sublayer i and increases according to parameter a.

Moreover, we should draw the reader's attention to the fact that, with a constant target efficiency for the absorbing layer (a given δ), the number of sublayers N increases with the decrease of the damping step parameter a. So, it is important to achieve a compromise for previous parameters so as to conserve a moderate total thickness e while avoiding spurious reflections due to a too strong increase of the damping ratio ξ in the thickness of the absorbing layer.

4. Numerical examples

In the following numerical applications, non-harmonic waves will be investigated by considering a Ricker incident wave *Ric* defined by:

$$Ric(t,\, t_\mathrm{p},\, t_\mathrm{s}) = A\left(2\pi^2 \frac{(t-t_\mathrm{s})^2}{t_\mathrm{p}^2} - 1\right) \exp\left(-\pi^2 \frac{(t-t_\mathrm{s})^2}{t_\mathrm{p}^2}\right) \tag{52}$$

The Ricker wave is characterized by three parameters: the fundamental period t_p, the time shift t_s and the amplitude A. The chosen values are: $t_\mathrm{p} = 3$ s, $t_\mathrm{s} = 3$ s and $A = 1$, as illustrated in Fig. 5.

The first example deals with a 1D non-harmonic wave propagation in the damping Rayleigh medium. The numerical solution obtained from a Finite Element Analysis using an implicit time integration is validated against the reference results obtained by Discrete Fourier Transform and Discrete Inverse Fourier Transform using Matlab software. Then, it will be shown that the condition in Eq. (45) minimizes the reflected waves by computing the wave propagation through the interface between an elastic medium and a damping Rayleigh medium. Finally, in order to assess the effectiveness of the proposed absorbing layer, the 2D Lamb test is simulated: a load force is applied to the surface of a 2D mesh and displacements are recorded at a given point also located at the surface of the mesh. The simulation will be conducted by coupling two finite-element codes with different time steps: explicit FE code Europlexus for the domain of interest coupled with implicit FE code Cast3m for the Rayleigh damping layer using an external coupling software (Brun et al. [5]).

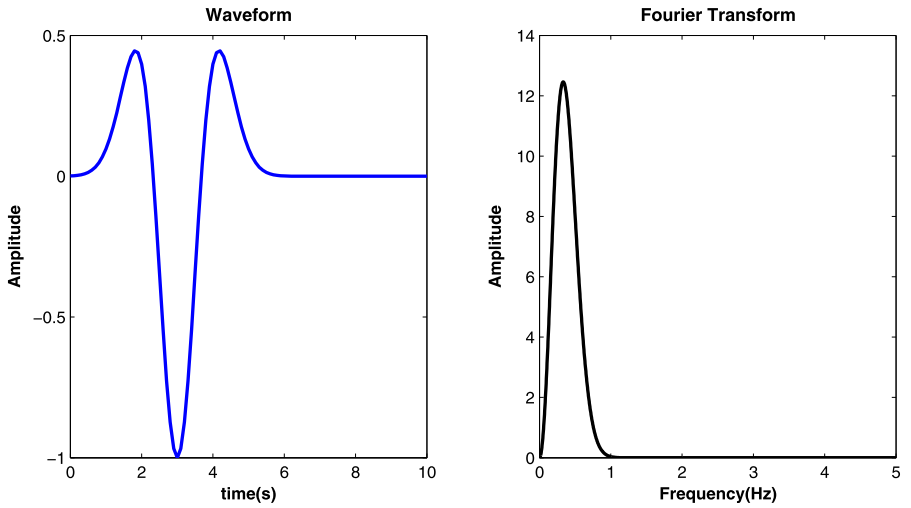

Fig. 5. (Color online.) Waveform and Fourier transform of the Ricker wavelet.

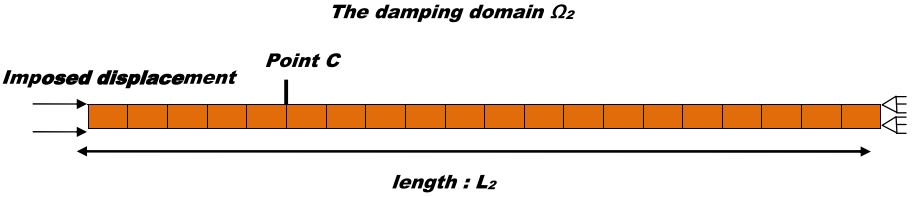

Fig. 6. (Color online.) Homogeneous damping layer of length 5λ.

4.1. 1D wave propagation in the Rayleigh damping material

In this example, we consider a problem of P-waves. The solution given by the finite-element method will be computed using Cast3m software [13].

The material properties are: $E = 10$ MPa, $\nu = 0.24$, $\rho = 1700$ kg/m^3 for Young's modulus, Poisson's ratio and mass density. A uniform finite-element mesh of four-node rectangular elements with linear shape functions is set up as shown in Fig. 6. The size of each finite element is equal to $\frac{\lambda}{50}$, where $\lambda = V_{1p}t_p = 230$ m. The displacement is prescribed at the left end of the mesh at point $x = 0$ according to the previous Ricker wavelet. The total size of the mesh extends to a distance of 5λ. The mesh is chosen to be very large so as to avoid the interference between the incident wave and the reflected wave, which propagates back towards the displacement-imposed point. An implicit time integration scheme is adopted (constant acceleration scheme).

Finally, the displacement is recorded at a point C located at 0.4λ from the end left of the mesh. In Fig. 7, the predicted displacement at point C is compared with the analytical solution for 1D wave propagating in 1D Rayleigh medium.

Fig. 7 presents the displacement ratio ($\frac{\tilde{u}_2(x,t)}{A}$) computed at point C using Cast3m and Matlab (reference results) against the solution without damping ($\xi = 0$), also computed using Matlab. It can be checked that the numerical and analytical results with $\xi = 0.5$ and $\xi = 1$ match quite well.

By varying the damping factor ξ, the numerical logarithmic decrement $\delta^{\text{num}} = f(\xi)$ at the recording point C is computed and compared with the approximate formula in Eq. (38) obtained for harmonic waves. From this comparison displayed in Fig. 8, it can be observed that the approximate formula is a good estimation for non-harmonic waves such as the Ricker wave by a dominant frequency.

4.2. 1D wave propagation from an elastic medium towards the Rayleigh damping medium separated by an interface

In order to validate the theoretical results obtained in Section 3.2, we start by considering the problem illustrated in Fig. 9.

The characteristics of the two materials are summarized in Table 1.

We impose the displacement at point $x = -5\lambda$ according to the same Ricker wave as previously described. Then, we compute the displacement at point C located at 0.4λ from the imposed displacement point. Here we can observe that point C is far enough from the interface $x = 0$ to avoid the interference between the reflected wave and the incident wave. The Young modulus of subdomain 2, as given in Table 1, is dependent on the damping ratio as: $\gamma = \frac{1}{\sqrt{1+\xi^2}}$. Fig. 10 displays

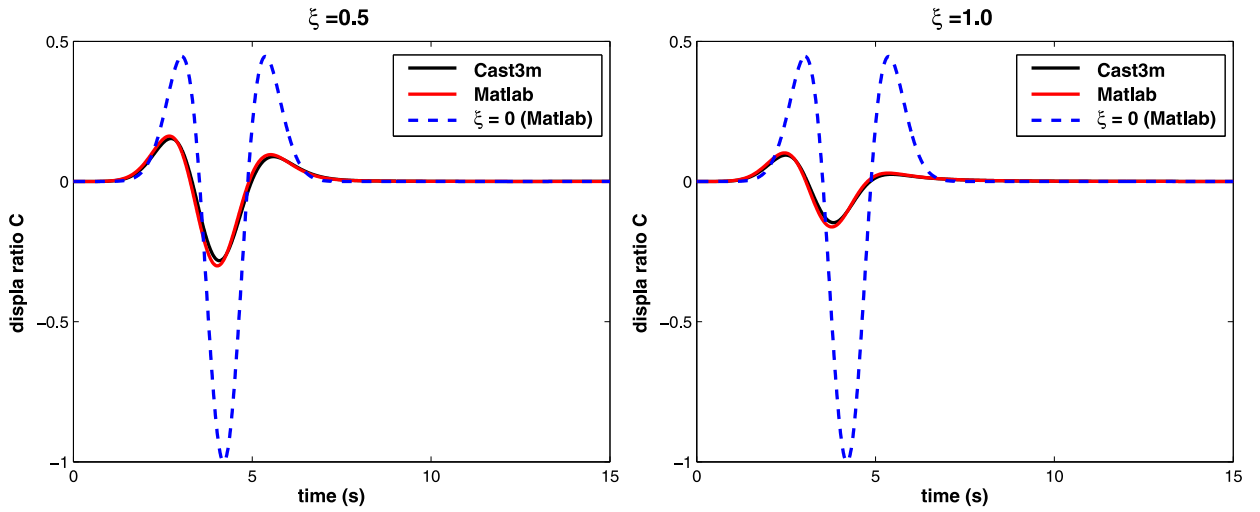

(a) ξ=0.5 (b) ξ=1.0

Fig. 7. (Color online.) Displacement at point C, $\omega_0 = \frac{2\pi}{t_p} = 2.09$ rad/s, $\xi = 0.5$ (left), $\xi = 1$ (right).

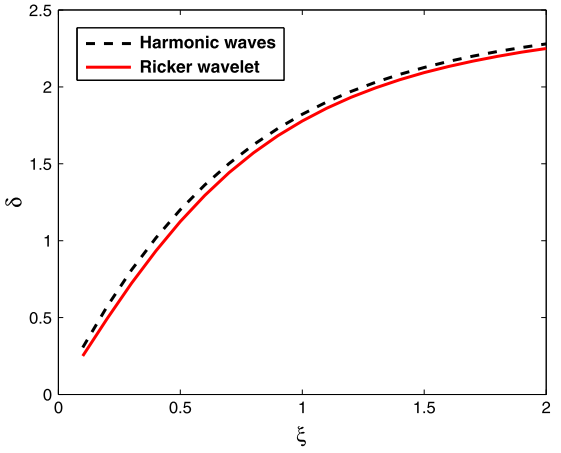

Fig. 8. (Color online.) Evolution of the logarithmic decrement δ^{num} at point C as a function of ξ for a Ricker wavelet: comparison with the theoretical curve valid for harmonic waves.

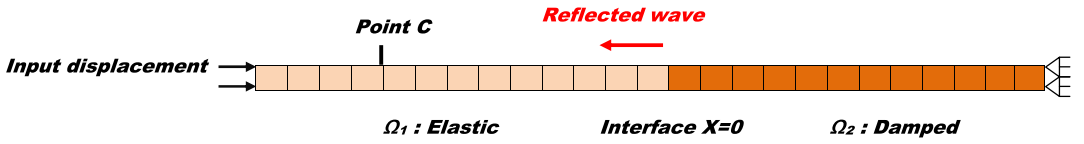

Fig. 9. (Color online.) The geometrical characteristics of the mesh.

Table 1
Characteristics of the materials.

	Subdomain 1 (Hooke material)	Subdomain 2 (damping material)
Young's modulus (MPa)	10	Variable
Poisson's ratio	0.24	0.24
Element size	$\frac{\lambda}{50}$	$\frac{\lambda}{50}$
Type of element	Rectangular (linear)	Rectangular (linear)
Mesh length	5λ	5λ
Mass density (kg/m^3)	1700	1700

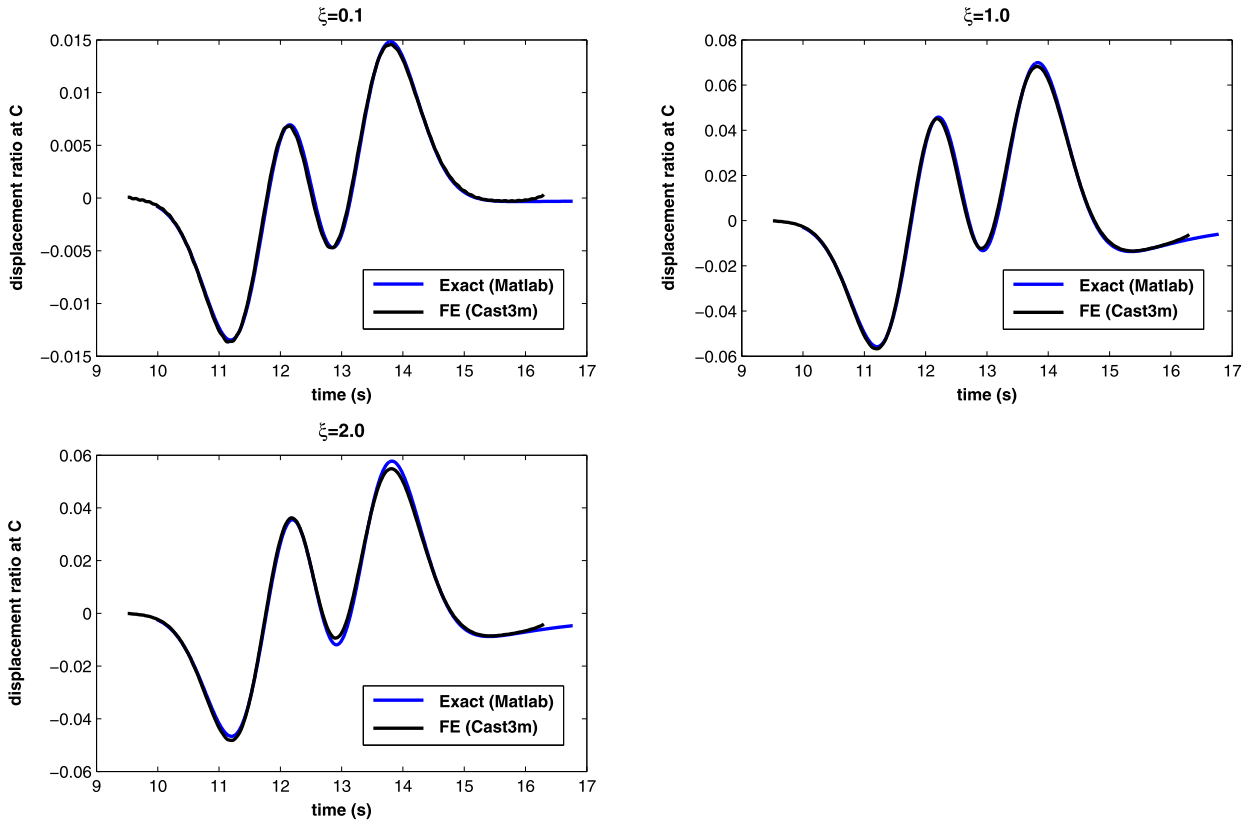

Fig. 10. (Color online.) Reflected wave computed at point C, $\omega_0 = \frac{2\pi}{t_p} = 2.09$ rad/s.

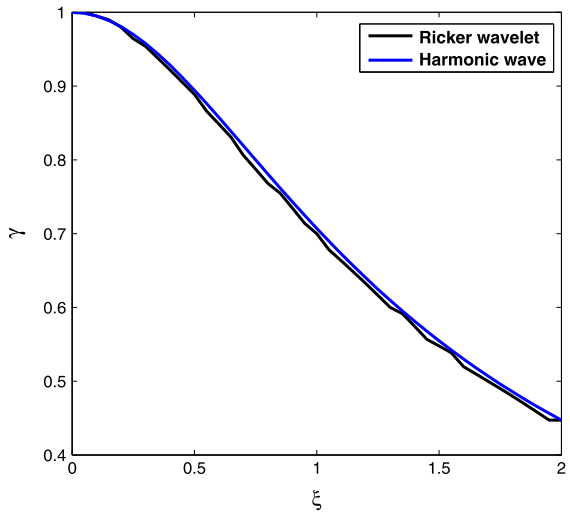

Fig. 11. (Color online.) Values of γ minimizing the amplitude of the reflected waves: theoretical curve with harmonic waves ($\gamma = \frac{\rho_2 V_2}{\rho_1 V_1} = \frac{1}{\sqrt{1+\xi^2}}$) and identified numerical curve considering a Ricker wave.

the comparison of results between the FE method using Cast3m with an implicit time integration scheme and the reference results using Matlab for several values of ξ.

From Fig. 10, it can be checked that both curves (numerical and analytical results) are in very good agreement for different values of ξ. In the first case, $\xi = 0.1$; the wave is reflected with a ratio of 1.5%, which is much lesser than the other cases: 5.5% for $\xi = 1$ and 6% for $\xi = 2$. It is worth noting that in all cases, the relationship given in Eq. (46) between

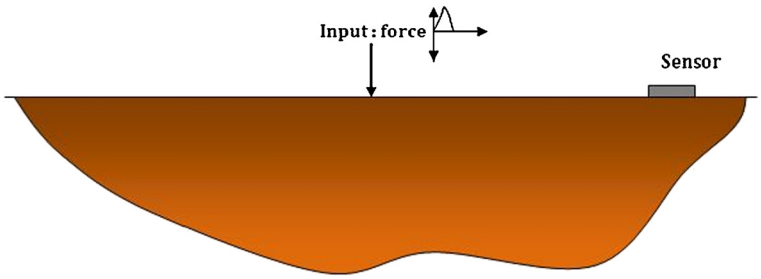

Fig. 12. (Color online.) Lamb test.

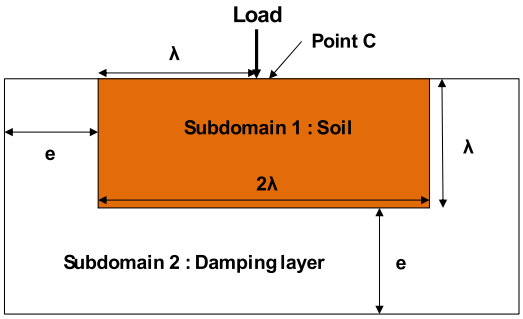

Fig. 13. (Color online.) Split domain into two subdomains: the domain of interest and the damping layer.

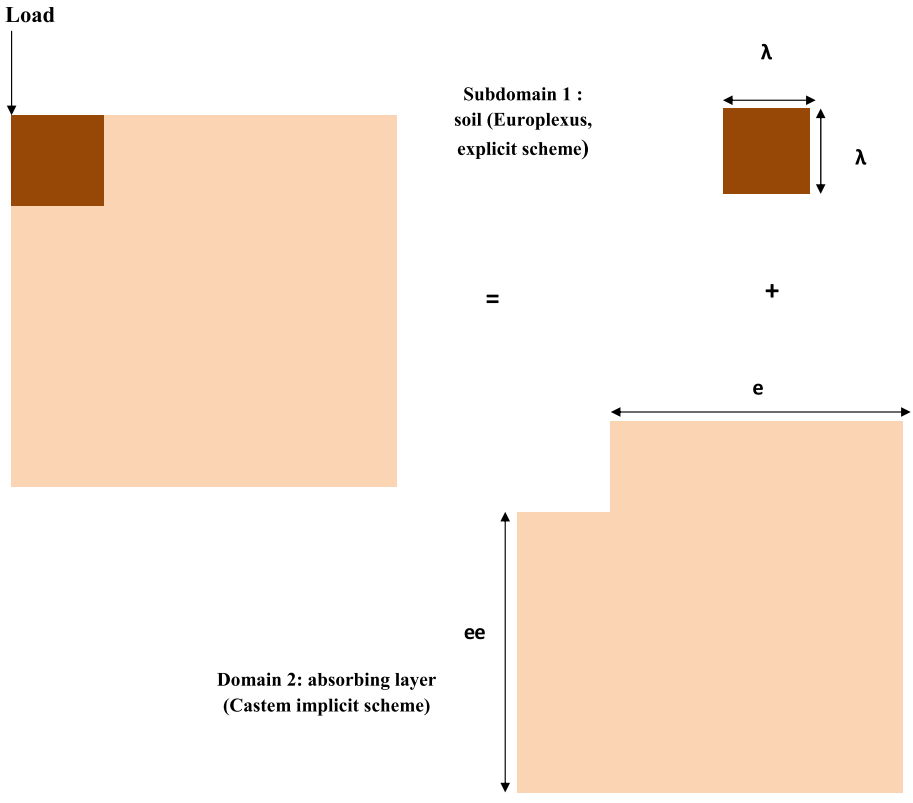

Fig. 14. (Color online.) The coupled problem: subdomain 1 (soil) modeled by Europlexus and subdomain 2 (absorbing medium) modeled by Cast3m.

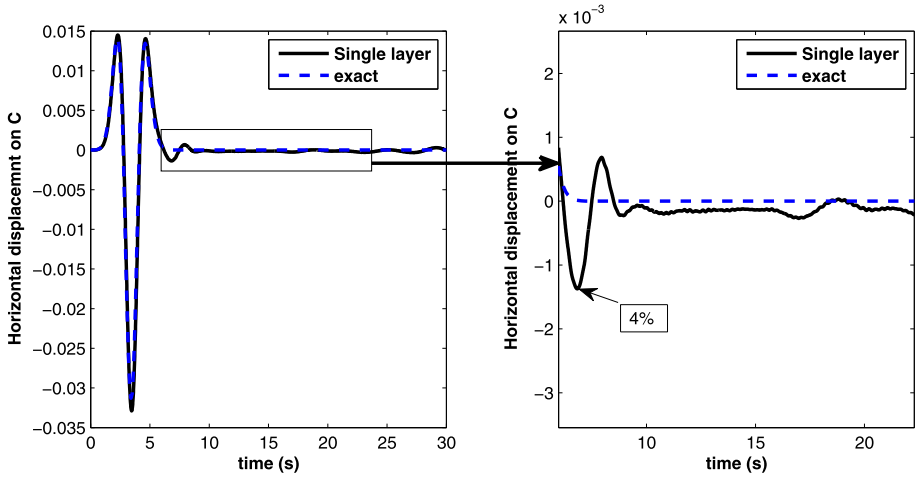

(a) Horizontal displacement

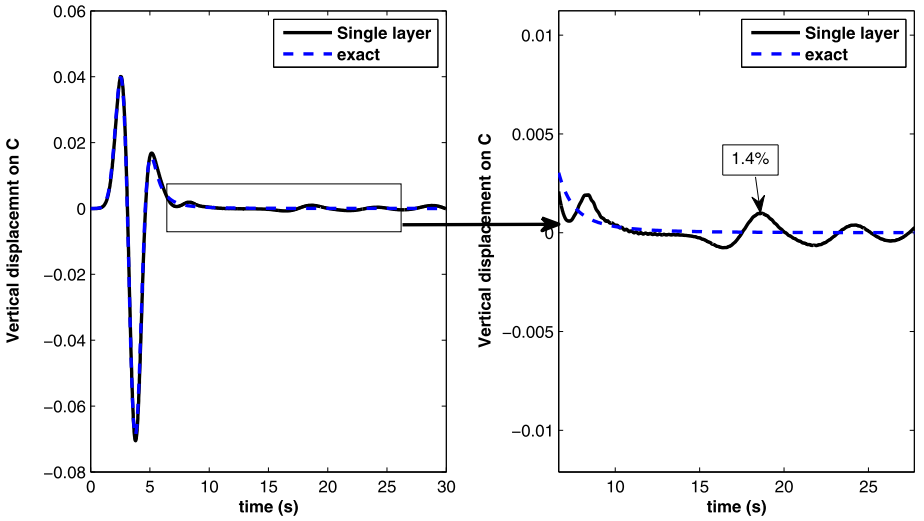

(b) Vertical displacement

Fig. 15. (Color online.) Horizontal and vertical displacements plotted at point C: analytical results (Lamb) versus numerical results using a Raleigh damping medium.

the material parameters of the two subdomains is satisfied. In the case of a homogeneous Young modulus for the two subdomains, the level of reflected waves is much higher: 2%, 20% and 40% for $\xi = 0.1$, $\xi = 1$ and $\xi = 2$, respectively.

Without imposing the relationship between the material parameters, we study the effect of a varying Young modulus E_2 in the damping layer. All the other parameters are kept constant, that is Poisson's coefficient and density. For a given damping ratio ξ, the Young modulus that minimizes the amplitude of reflected waves has been identified. Then the ratio $\gamma_{\text{num}} = \frac{\rho_2 V_2}{\rho_1 V_1}$ has been computed for a given value of the damping ratio. Over a range of damping ratios varying from 0 to 2, the optimized ratio $\frac{\rho_2 V_2}{\rho_1 V_1}$ is plotted versus the damping ratio in Fig. 11 and compared with the previous theoretical relationship, i.e. $\gamma(\xi) = \frac{1}{\sqrt{1+\xi^2}}$. It can be seen that the numerical identified curve matches very well the theoretical curve. It is important to note that the condition $\gamma(\xi) = \frac{1}{\sqrt{1+\xi^2}}$ for minimizing the reflected waves at the interface has been obtained only for harmonic waves and for the 1D wave propagation case. From Fig. 11, it can be concluded that this condition provides an excellent approximation for non-harmonic waves such as the Ricker wave.

4.3. 2D Lamb's test using explicit/implicit multi-time step co-computations

Lamb's test consists in applying a concentrated load to the surface of a ground assumed to be infinite in both directions. A sensor is located at a distance $d = 10$ m from the load point in order to record the vertical and the horizontal

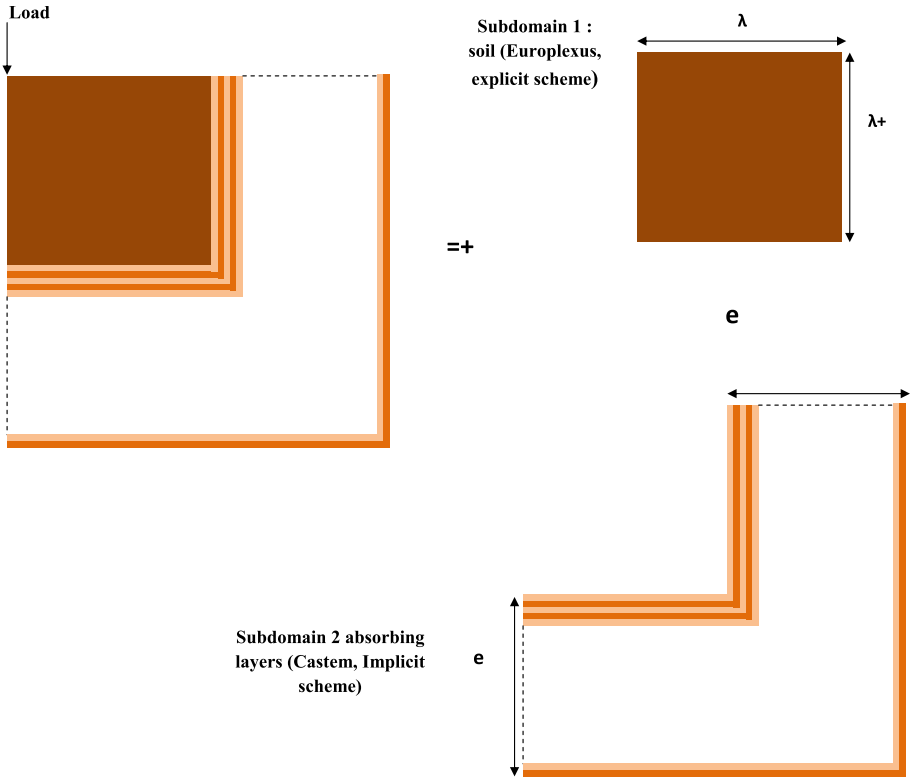

Fig. 16. (Color online.) FE model for subdomains 1 (soil) and 2 (multi-layered damping medium).

displacements at this point (Fig. 12). In 1904, Lamb [11] analytically calculated the displacements at a given point of the surface by assuming an isotropic linear elastic behavior for the soil. The derived theoretical solution exhibits the complexity of the problem, since there are many types of waves traveling through the soil (P- and S-waves, Rayleigh waves, *etc.*). In this part, we will compute the numerical solution using the multi time step explicit/implicit GC method. Two FE codes are involved into the co-computations: Europlexus code [2] based on a explicit time integration scheme for the domain of interest associated with a fine time step and implicit Cast3m code [13] for the damping layers associated with a large time step.

The rest of this section will be divided into two parts: the first one will be devoted to the analysis of the accuracy by comparing the numerical and the analytical results using both multi-layer and single-layer strategies. Here the fine time step will be adopted for the explicit subdomain, satisfying the CFL condition. Furthermore, we will show that the multilayer strategy gives a better accuracy with a mesh drastically reduced compared to the single-layer strategy. In the second part, we will study the effect of the time step ratio on the accuracy by varying the time step of the damping domain. In this study on the effect of the time step ratio, the multi-layer strategy is again employed, with the same parameters as in the previous part.

4.3.1. The single- and the multi-layer strategy in Lamb's test with a homogeneous time step

In Fig. 13, the split domain is illustrated: subdomain 1 models the soil assumed to be linear elastic with $\rho_1 = 1700\ \text{kg/m}^3$, $E_1 = 10$ MPa and $\nu_1 = 0.24$, and subdomain 2 models the Rayleigh damping medium with $\rho_2 = 1700\ \text{kg/m}^3$ and $\nu_2 = 0.24$. The Rayleigh matrix has the following parameters: $\xi = 0.1$ and $\omega_0 = \frac{2\pi}{t_p}$ according to Eq. (36). The soil is modeled by a rectangle surrounded by the damping layer of thickness e. A concentrated load is applied to the middle of the surface, defined by a Ricker wave with the parameters $A = 1MN$, $t_p = 3$, $t_s = 3$. Fig. 14 presents the meshes used for this simulation, the soil is modeled by Europlexus code (the symmetry is taken into account) using rectangular elements with size of $\frac{\lambda}{50}$ and the Rayleigh damping medium is modeled by Cast3m code using the same size of elements as in subdomain 1.

The damping layer is defined by a target logarithmic decrement $\delta = \ln(10)$, leading to a thickness $e = 914\ \text{m} = 4\lambda$ by using the design thickness equation in Eq. (38). It is worth noting that this logarithmic decrement targets 90% of amplitude decay of the incident way for one-way up to the end of the damping layer. Same decay occurs for the reflected wave at the end of the damping layer, thus the incident wave is globally decreased by 99%. So the target logarithmic decrement of $\delta = \ln(10)$ corresponds to a ratio of 0.01 between the amplitudes of the reflected wave coming from the end of the damping layer and that of the incident wave.

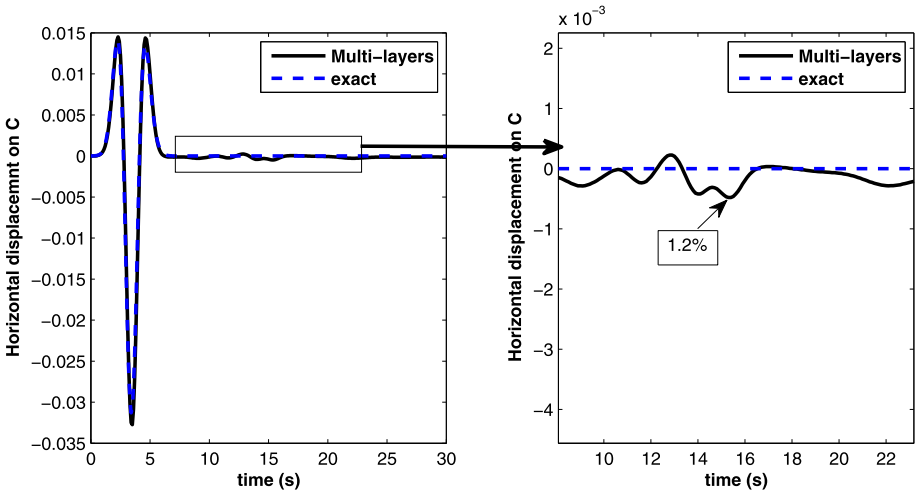

(a) Horizontal displacement

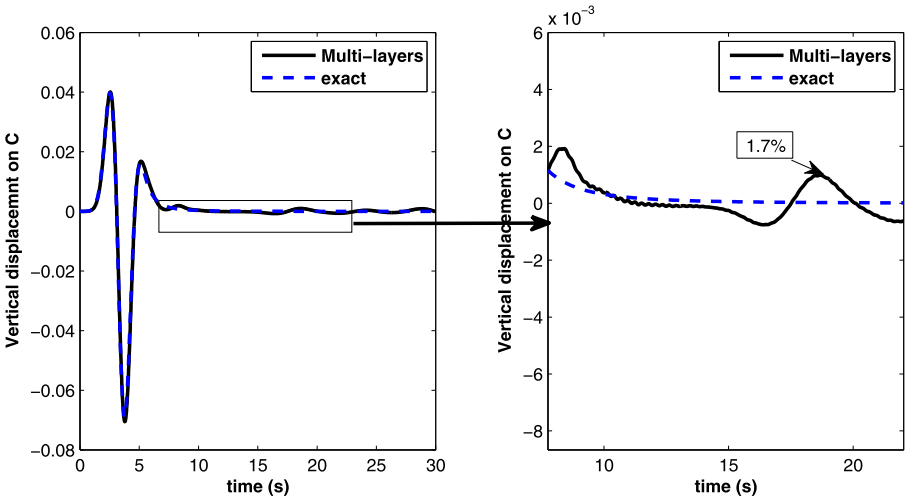

(b) Vertical displacement

Fig. 17. (Color online.) Vertical and horizontal displacements plotted at point C: the red curves correspond to the reference results and the blue ones correspond to the method using several layers.

A point C, located at 10 m from the load point, is chosen for recording the horizontal and vertical displacements.

In Fig. 15, the results computed at point C using the Rayleigh damping layer are compared with Lamb's analytical solutions using Matlab. It can be highlighted that our explicit/implicit strategy with a Rayleigh damping layer provides numerical results in acceptable agreement with respect to the reference solution, despite the fact that there are small reflections observed at $t = 8$ s less than 4% of the incident wave (horizontal displacement in Fig. 15). Consequently, it has been shown that the approximate condition in Eq. (45) enables to efficiently minimize the reflected waves at the interface in this 2D case involving non-harmonic waves and angled incidence, although this condition has been obtained for harmonic waves with a normal incidence.

In order to reduce the size of the damping medium, we propose to replace the previous global layer by several sublayers, each one satisfying the conditions detailed in Section 3.2. Fig. 16 shows the detail of the mesh used for this simulation, the first subdomain, which represents the soil, is still modeled by Europlexus software using the explicit time integration scheme and the second subdomain is divided into several sublayers modeled by Cast3m using the implicit scheme. The same characteristics are used for the soil as in the previous example.

The thickness of each sublayer, as mentioned in Section 3.3, is equal to the element size $h = \frac{\lambda}{50}$. The design of the absorbing layer is governed by the system in Eq. (51): a damping ratio step a equal to 2% is selected, with a first damping ratio ξ_1 equal to 2%. Considering a target value of $\delta = \ln(10)$ for the logarithmic decrement in the thickness of the absorbing layer, we obtain a total number of sublayers N equal to 40.

Fig. 17 compares the displacements computed at the same point C corresponding to the reference results (Lamb's solutions) and the Rayleigh damping with several sublayers. It can be underlined that a better accuracy is achieved using the

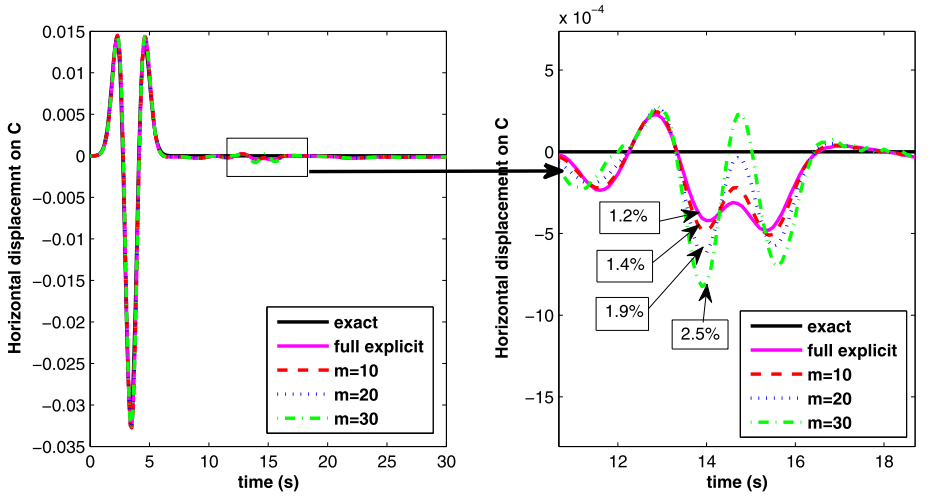

(a) Horizontal displacement

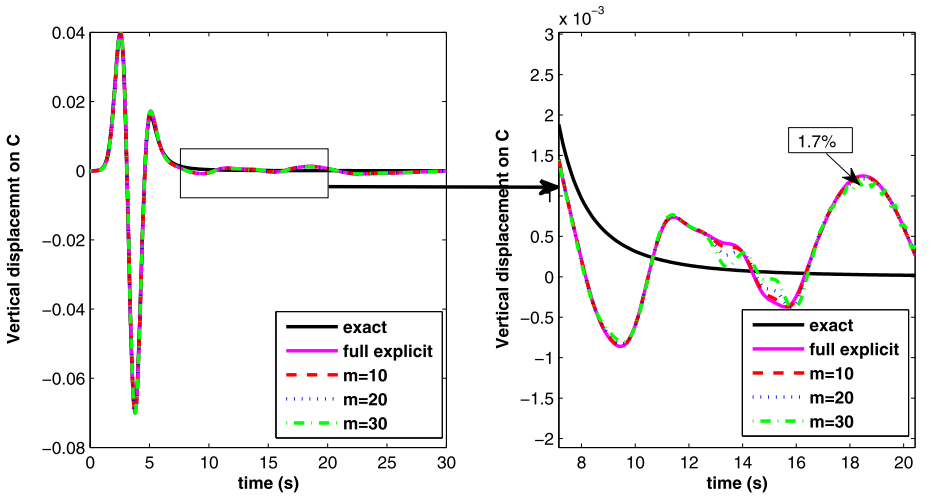

(b) Vertical displacement

Fig. 18. (Color online.) Horizontal and vertical displacements plotted at point C: analytical results (Lamb) versus numerical results using a Raleigh damping medium for different time step ratios.

multi-layer strategy with a spurious reflected wave with an amplitude of less than 1% with respect to the amplitude of the incident wave. Considering that the thickness of the absorbing layer is reduced from 3.6λ to 0.8λ, the efficiency of the multi-layer strategy is highlighted.

4.3.2. Effect of the time ratio for the multi-layer strategy

As demonstrated by the authors, the GC method dissipates energy at the interface due to the heterogeneity of the time steps between the subdomains. Hence, it is crucial to quantify the discrepancies by varying the time step ratio and comparing the numerical and the reference results. Since the damping layers are integrated by an implicit scheme, it is interesting to increase the time step of this subdomain through the time ratio m defined as $\frac{\Delta t_2}{\Delta t_1} = 10, 20,$ and 30. All numerical results computed for different values of m will be compared to the exact solution and numerical results computed using only the explicit scheme for the whole problem (soil and damping layers). Furthermore, we keep the same physical properties as the previous section for the both subdomains.

In Fig. 18, the horizontal and vertical displacements recorded at the same point C are compared to the displacements given by a full-explicit computation and the analytical solutions. Here, we observe that the error in horizontal displacement increases with the time step ratio up to a maximum value of 2.5%, while the error in vertical displacement is approximately equal to 1.7%. We remind that our target in the beginning was to reach an error at about 1%. From Fig. 18, it can be noted that the discrepancy between the full-explicit computation and the theoretical Lamb solution is equal to 1.2% for horizontal displacement. Adopting different time integrators (explicit/implicit) with their own time step leads to a slight additional

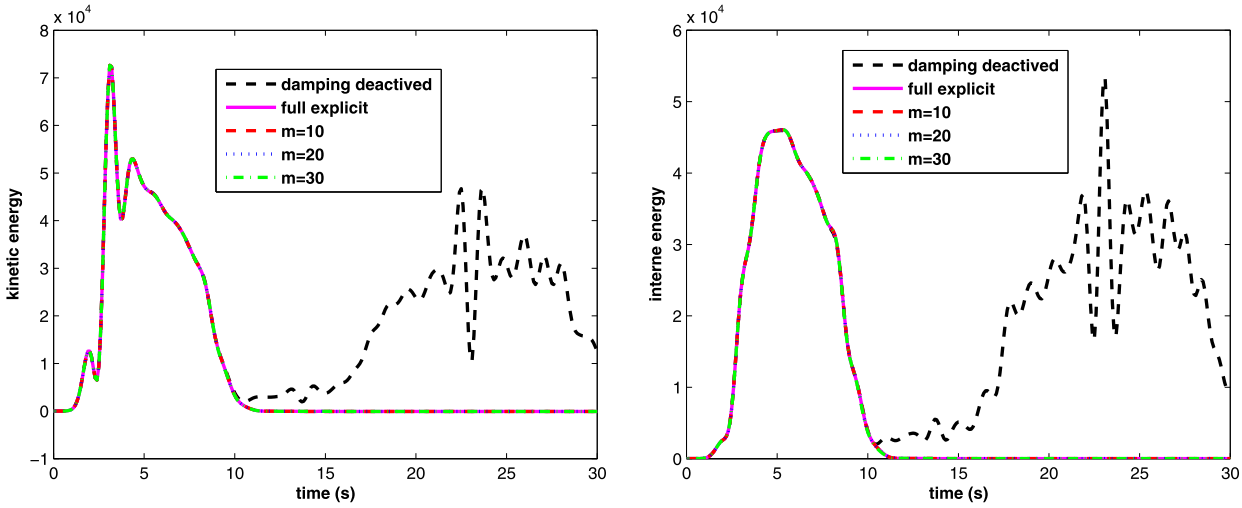

(a) kinetic energy (b) internal energy

Fig. 19. (Color online.) Kinetic and internal energies computed for different values of the time step ratio m.

Table 2
Relative errors for several values of m.

	Kinetic energy	Internal energy
$m = 10$	0.04%	0.02%
$m = 20$	0.1%	0.08%
$m = 30$	0.3%	0.15%

discrepancy of about 1.5%. Thus the multi time step ability of the GC method is of great interest for the purpose of reducing the computation time related to the introduction of the absorbing layers.

In Fig. 19, the kinetic and internal energies are computed for different time step ratios. The case with a zero damping ratio ($\xi = 0$) in the subdomain corresponding to the absorbing layers (see Fig. 16) is added so as to highlight the coming back energy when the dissipating property of the multi layer is deactivated. The error in terms of kinetic and internal energy is defined by: $err = \frac{\|E_{\mathrm{I/E}}^{(m)} - E_{\mathrm{ref}}\|_{L^2([0,T])}}{\|E_{\mathrm{ref}}\|_{L^2([0,T])}}$, where $E_{\mathrm{I/E}}^{(m)}$ denotes the kinetic or internal energy obtained using multi-time step co-computations with the time step ratio m and E_{ref} is the reference energy (kinetic or internal) obtained from the full-explicit computation. From Table 2, it can be noted that the error in kinetic energy increases from 0.04% to 0.3% when increasing the time step ratio from 10 to 30, whereas the error in internal energy increases from 0.02% to 0.13%. It can be concluded that the size of the time step ratio has a small effect on the efficiency of the multi-layer strategy, enabling large gain in terms of computation time to be achieved.

5. Conclusion

The proposed procedure for designing an efficient absorbing layer aims at optimizing the Rayleigh absorbing layers and the use of modern subdomain coupling approach enabling to select heterogeneous time integrators with their own time step depending on subdomains.

First, a strong form for wave propagation in a damping Rayleigh medium is given. It has been shown that the proposed strong form exactly corresponds to the introduction of the Rayleigh matrix into the discretized equation of motion by the finite-element method. The strong form is then used with a view to studying the wave propagation through an interface between two media with different elastic parameters. It provides optimal conditions for minimizing the reflected waves generated at the interface. A procedure for designing absorbing layer is set up by targeting a performance criterion expressed in terms of logarithmic decrement in the layer thickness. A compromise has to be achieved: optimizing the damping of the incident waves in the layer thickness while reducing the spurious waves at the interface.

Secondly, a subdomain coupling method is employed, enabling us to select an appropriate time integrator for the absorbing layer with a large time step, while adopting an explicit time integration scheme for the domain of interest with a fine time step satisfying the CFL condition. Multi time step explicit/implicit co-computations involving two FE codes have been successfully carried out. Two strategies are investigated: an absorbing layer with a constant damping ratio and an absorbing layer composed of a series of sublayers with increasing damping ratios.

The numerical results are compared to the analytical results in 1D and 2D wave propagation problems with non-harmonic waves (Ricker wavelet). The proposed procedure for the design of an absorbing layer combined with a subdomain coupling approach turns out to be efficient for reproducing unbounded media.

The next stage of this work is to couple perfect match layers and heterogeneous multi-time step subdomain techniques.

References

[1] Cast3m, Présentation et utilisation de Cast3m, 2011.
[2] Europlexus, User's manual, 2006.
[3] U. Basu, A. Chopra, Perfectly matched layers for time-harmonic elastodynamics of unbounded domains: theory and finite-element implementation, Int. J. Numer. Methods Biomed. Eng. 192 (2003) 1337–1375.
[4] P. Bettess, Infinite elements, Int. J. Numer. Methods Biomed. Eng. 11 (1977) 53–64.
[5] M. Brun, A. Batti, A. Limam, A. Combescure, Implicit/explicit multi-time step co-computations for predicting reinforced concrete structure response under earthquake loading, Soil Dyn. Earthq. Eng. 33 (2012) 19–37.
[6] M. Brun, A. Batti, A. Combescure, A. Gravouil, External coupling software based on macro- and micro-time scales for explicit/implicit multi-time-step co-computations in structural dynamics, Finite Elem. Anal. Des. 86 (2014) 101–119.
[7] A. Combescure, A. Gravouil, A numerical scheme to couple subdomains with different time-steps for predominantly linear transient analysis, Comput. Methods Appl. Mech. Eng. 191 (2002) 1129–1157.
[8] B. Enquist, A. Majda, Absorbing boundary conditions for the numerical simulation of waves, Math. Comput. 31 (1977) 629–651.
[9] A. Gravouil, A. Combescure, A multi-time-step explicit–implicit method for non-linear structural dynamics, Int. J. Numer. Methods Biomed. Eng. 50 (2001) 199–225.
[10] T. Hughes, The Finite Element Method: Linear Static and Dynamic Finite Element Analysis, Prentice-Hall, Englewood Cliffs, NJ, 1987.
[11] H. Lamb, On the propagation of tremors over the surface of an elastic solid, Proc. R. Soc. Lond. 72 (1903) 128–130.
[12] K. Meza-Fajardo, A. Papageorgiou, A nonconvolutional, split-field, perfectly matched layer for wave propagation in isotropic and anisotropic elastic media: stability analysis, Bull. Seismol. Soc. Am. 98 (2008) 1811–1836.
[13] A. Millard, CASTEM 2000, Manuel d'utilisation, Rapport CEA-LAMBS, No. 93/007. CEA-LAMBS, Saclay, Paris, 1993.
[14] P. Rajagopal, M. Drozdz, E.A. Skelton, M.S. Lowe, R.V. Craster, On the use of the absorbing layers to simulate the propagation of elastic waves in unbounded isotropic media using commercially available finite element packages, Nondestruct. Test. Eval. Int. 51 (2012) 30–40.
[15] J.-F. Semblat, Rheological interpretation of Rayleigh damping, J. Sound Vib. 338 (1997) 741–744.
[16] J.-F. Semblat, L. Lenti, A. Gandomzadeh, A simple multi-directional absorbing layer method to simulate elastic wave propagation in unbounded domains, Int. J. Numer. Methods Biomed. Eng. 85 (2011) 1543–1563.
[17] J.P. Wolf, Dynamic Soil–Structure Interaction, Prentice-Hall, Englewood Cliffs, NJ, 1985.